



## *In-vitro* evaluation studies of 7-chloro-4-aminoquinoline Schiff bases and their copper complexes as cholinesterase inhibitors

Vanessa S. Zanon<sup>a</sup>, Josélia A. Lima<sup>b,c</sup>, Teobaldo Cuya<sup>d</sup>, Flavia R.S. Lima<sup>e</sup>, Anna C.C. da Fonseca<sup>e</sup>, Javier G. Gomez<sup>a</sup>, Ronny R. Ribeiro<sup>f</sup>, Tanos C.C. França<sup>c</sup>, Maria D. Vargas<sup>a,\*</sup>

<sup>a</sup> Instituto de Química, Universidade Federal Fluminense, Campus do Valonguinho, 24020-141 Niterói, RJ, Brazil

<sup>b</sup> Departamento de Química Orgânica, Instituto de Química, Universidade Federal do Rio de Janeiro, 21941-909 Rio de Janeiro, RJ, Brazil

<sup>c</sup> Laboratório de Modelagem Aplicada a Defesa Química e Biológica (LMDQB), Instituto Militar de Engenharia, 22290-270 Rio de Janeiro, RJ, Brazil

<sup>d</sup> Faculdade de Tecnologia, Departamento de Matemática, Física e Computação, Universidade do Estado do Rio de Janeiro, 27537-000 Resende, RJ, Brazil

<sup>e</sup> Laboratório de Biologia das Células Gliais, Instituto de Ciências Biomédicas, Centro de Ciências da Saúde, Universidade Federal do Rio de Janeiro, 21941-902 Rio de Janeiro, RJ, Brazil

<sup>f</sup> Departamento de Química, Universidade Federal do Paraná, CP 19081, 81531-990 Curitiba, PR, Brazil

### ARTICLE INFO

#### Keywords:

Alzheimer's disease  
Schiff bases  
Molecular modeling  
4-Aminoquinolines  
Copper complexes  
Acetylcholinesterase inhibition activity

### ABSTRACT

Alzheimer's disease (AD) is one of the most common age-related neurodegenerative disorders. Aggregation of amyloid- $\beta$  peptide into extracellular plaques with incorporation of metal ions, such as  $\text{Cu}^{2+}$ , and reduction of the neurotransmitter acetylcholine levels are among the factors associated to the AD brain. Hence, a series of 7-chloro-4-aminoquinoline Schiff bases (**HLa-e**) were synthesized and their cytotoxicity and anti-cholinesterase activity, assessed for Alzheimer's disease. The intrinsic relationship between  $\text{Cu}^{2+}$  and the amyloidogenic plaques encouraged us to investigate the chelating ability of **HLa-e**. Dimeric tetracationic compounds,  $[\text{Cu}_2(\text{N}^{\text{H}}\text{La-e})_4]\text{Cl}_4$ , containing quinoline protonated ligands were isolated from the reactions with  $\text{CuCl}_2 \cdot 2\text{H}_2\text{O}$  and fully characterized in the solid state, including an X ray diffraction study, whereas EPR data showed that the complexes exist as monomers in DMSO solution. The inhibitory activity of all compounds was evaluated by Ellman's spectrophotometric method in acetylcholinesterase (AChE) from *Electrophorus electricus* and butyrylcholinesterase (BChE) from equine serum. **HLa-e** and  $[\text{Cu}(\text{N}^{\text{H}}\text{Ld})_2]\text{Cl}_2$  were selective for AChE ( $\text{IC}_{50} = 4.61\text{--}9.31 \mu\text{M}$ ) and were not neurotoxic in primary brain cultures. Docking and molecular dynamics studies of **HLa-e** inside AChE were performed and the results suggested that these compounds are able to bind inside AChE similarly to other AChE inhibitors, such as donepezil. Studies of the affinity of **HLD** for  $\text{Cu}^{2+}$  in DMSO/HEPES at pH 6.6 and pH 7.4 in  $\mu\text{M}$  concentrations showed formation of analogous 1:2  $\text{Cu}^{2+}$ /ligand complexes, which may suggest that in the AD-affected brain **HLD** may scavenge  $\text{Cu}^{2+}$  and the complex, also inhibit AChE.

### 1. Introduction

Alzheimer's disease (AD) is an age-related neurodegenerative progressive and fatal disorder, whose etiology is still unknown. It has affected 50–60% of the over 46 million people worldwide living with dementia in 2015 and this number is expected to double every twenty years [1]. The etiology of AD is still unknown. The main features in the brain with AD are extracellular deposits of insoluble amyloid- $\beta$  ( $\text{A}\beta$ ) plaques and abnormal aggregation of hyperphosphorylated tau protein into intracellular neurofibrillary tangles [2]. These two neuronal conditions have been associated with drastic reduction of the synthesis [3], storage and release of the neurotransmitter acetylcholine (ACh) [4],

affecting learning and memory processes [5].

For decades, researchers have been trying to understand AD by addressing some therapeutic targets, such as the  $\text{A}\beta$  aggregation process [6], tau phosphorylation, acetylcholinesterase inhibition, secretase enzymes modulation, oxidative stress, etc. Still, currently available drugs for palliative treatment of AD are cholinesterase reversible inhibitors (ChEI), such as galantamine, tacrine, rivastigmine and donepezil, and the *N*-methyl-D-aspartate (NMDA) antagonist memantine [7]. Tacrine, a quinoline derivative, was the first drug approved by the US Food and Drug Administration (FDA) to treat AD in 1991. In spite of the benefits offered by the treatment with this drug, its use was discontinued in the US in 2013 because of serious side effects, including hepatotoxicity [8].

\* Corresponding author.

E-mail address: [mdvargas@id.uff.br](mailto:mdvargas@id.uff.br) (M.D. Vargas).

<https://doi.org/10.1016/j.jinorgbio.2018.11.019>

Received 6 June 2018; Received in revised form 26 November 2018; Accepted 27 November 2018

Available online 30 November 2018

0162-0134/ © 2018 Published by Elsevier Inc.

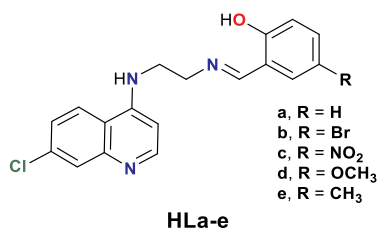


Fig. 1. Structures of compounds HLa-e.

Studies have been conducted aiming at a suitable replacement [9–12] and various tacrine analogues have been investigated in an attempt to reduce the side effects of this drug and increase efficiency [13,14].

In the healthy brain copper is mostly bound to copper enzymes or carrying proteins. A meta-analysis of studies on serum, plasma, and cerebrospinal fluid has confirmed higher copper levels in AD patients than in healthy controls [15]. Furthermore, in the AD brain evidence for a copper imbalance has been reported, with labile copper increase opposed to copper bound to proteins [16]. A large body of evidence suggests that  $\text{Cu}^{2+}$  bound to A $\beta$  is implicated in AD, and that the Cu–A $\beta$  complex is involved in reactive oxygen species (ROS) production ( $\text{H}_2\text{O}_2$ ,  $\text{OH}\cdot$ ). Thus, a cascade of events responsible for oxidative stress occurs causing irreversible neuronal damage [17]. Additionally, A $\beta$  can attract and activate microglia, leading to an aggregation of cells around these A $\beta$  deposits in the brain [18], culminating in the secretion of pro-inflammatory mediators, including Interleukin-1 beta (IL-1 $\beta$ ), Tumor Necrosis Factor alpha (TNF- $\alpha$ ), Interleukin-6, (IL-6) and cyclooxygenase-2 (COX2) expression, among others [19–21].

To this extend a series of 7-chloro-4-aminoquinoline Schiff bases (HLa-e, Fig. 1) was evaluated for its ability to inhibit acetyl and butyrylcholinesterases (AChE and BuChE) and bind the elevated serum copper, thus preventing A $\beta$  metal interactions and avoiding formation of toxic A $\beta$  deposits. These compounds have been previously investigated for their antiplasmodium activities [22,23]. To our knowledge, there is no report in the literature concerning the evaluation of compounds containing the 7-chloro-4-aminoquinoline nucleus for AD. Herein we report the AChE inhibitory activity of HLa-e (Fig. 1) and molecular docking, as well as studies of the interaction of the most promising compound of the series (HLd) with  $\text{Cu}^{2+}$ . Due to the intrinsic relationship between the presence of copper ions and AD these molecules were also reacted with  $\text{CuCl}_2\cdot 2\text{H}_2\text{O}$  to analyze the species that could be formed. The metal complexes were fully characterized in the solid state and in solution, and their AChE inhibitory activity was also investigated.

## 2. Experimental

### 2.1. Materials and instrumentation

4,7-Dichloroquinoline (97%), 5-bromo-2-hydroxybenzaldehyde (98%), ethane-1,2-diamine (99%), 2-hydroxy-5-methoxybenzaldehyde (98%), 2-hydroxy-5-methylbenzaldehyde (98%), 2-hydroxy-5-nitrobenzaldehyde (99%) and  $\text{CuCl}_2\cdot 2\text{H}_2\text{O}$  ( $\geq 99\%$ ) were purchased from Sigma-Aldrich, 2-hydroxybenzaldehyde was purchased from Merck ( $> 99\%$ ), triethylamine ( $\geq 99\%$ , Sigma-Aldrich) was distilled before use. All other reagents were purchased from Sigma-Aldrich or Vetec chemicals and were used without further purification. The precursor  $N^1$ -(7-chloroquinolin-4-yl)ethane-1,2-diamine was prepared by refluxing 4,7-dichloroquinoline with ethane-1,2-diamine [24] and its identity and purity were confirmed by mp, IR and  $^1\text{H}$  NMR spectroscopy [25,26]. Its synthesis and characterization data are available in Supplementary information (SI). The general synthetic procedure for the previously reported HLa-d [22,23] and novel HLe, and the characterization data are also available in SI. All compounds had their purity confirmed by elemental analysis and melting point (Table 1).

CHN elemental analyses were carried out using a Perkin-Elmer 2400 at Universidade de São Paulo (USP-SP), Brazil. NMR spectra were recorded on a Varian VNMRs ( $^1\text{H}$  at 500 or 300 MHz,  $^{13}\text{C}$  NMR at 125 or 75 MHz) with dimethyl sulfoxide- $d_6$  ( $\text{DMSO-}d_6$ ) as the solvent. FTIR spectra were measured using a Varian 600 FTIR spectrometer equipped with a Pike ATR Miracle accessory (diamond/ZnSe crystal, resolution:  $4\text{ cm}^{-1}$ ) at room temperature in the range between  $4000\text{ cm}^{-1}$  and  $600\text{ cm}^{-1}$  with 32 scans (Table S1 of the Supplementary information). UV-Vis – NIR spectra in the 300 nm – 1000 nm range were collected on a Varian Cary 50 spectrophotometer using DMSO spectroscopic grade as solvent (Table S2). X-band Electron Paramagnetic Resonance (EPR) spectra were obtained from solid samples and from DMSO solutions at 77 K on a Bruker EMX microX (Table S3). The EPR spectra were simulated by EasySpin 4.5.1 software package [27]. Values of molar conductance ( $\Omega^{-1}\cdot\text{cm}^2\cdot\text{mol}^{-1}$ ) of the complexes were measured at room temperature using freshly prepared DMSO solutions (1 mM) with a CG 853 conductivity meter (Schott GmbH, Germany) calibrated with KCl solution (Table S2). Electron spray mass spectrometry (ESI-MS) experiments were carried out in a Perkin Elmer SQ-300 mass spectrometer using MS-grade methanol as a solvent.

### 2.2. General method for the synthesis of complexes $[\text{Cu}_2(\text{N}^{\text{H}}\text{La-e})_4]\text{Cl}_4$

A solution of  $\text{CuCl}_2\cdot 2\text{H}_2\text{O}$  (0.125 mmol) in MeOH (3–5 mL) was added to a suspension of HLa-e (0.25 mmol) in MeOH (5–30 mL), stirred at  $45^\circ\text{C}$  for 30 min, and then at room temperature for 24 h. When necessary, water was added (0.5–3 mL) to help precipitation of the products that were filtered off, washed with  $\text{H}_2\text{O}$  and dried in a desiccator under vacuum (Table 1).

### 2.3. Crystal structure analysis

Crystals of complex  $[\text{Cu}_2(\text{N}^{\text{H}}\text{Ld})_4]\text{Cl}_4$  were obtained from the mother solution, which was left to evaporate slowly for 15 days. X-ray diffraction data were collected on a D8 venture diffractometer equipped with a CMOS (Complementary metal-oxide-semiconductor) detector type and Mo anode ( $\text{MoK}\alpha$  radiation,  $\lambda = 0.71073\text{ \AA}$ ). Intensity data were recorded by  $\varphi$  and  $\omega$  scans. The structure was solved using SHELXS [28] and refined by full-matrix least-squares method on F2 using SHELXL [29] in the OLEX2 [30,31] platform, however, large R1 and S values were obtained. Crystal pattern analysis revealed the presence of a twinned crystal that was treated using CELLNOW and TWINABS programs [32]. Also, large residual peaks were observed in the lattice, presumably crystallized solvent, that were modeled as water molecules. This last procedure does not improve the crystal structure reliability and the water molecules were deleted. PLATON/SQUEEZE program was used on the raw data to generate a new data set that remove the scattering contribution by solvent electron density [33]. All non-hydrogen atoms have been refined anisotropically. Hydrogen atoms were found at expected positions and by the end of the refinement, they were positioned using riding constraints. Crystallographic data for complex  $[\text{Cu}_2(\text{N}^{\text{H}}\text{Ld})_4]\text{Cl}_4$ :  $\text{C}_{38}\text{H}_{36}\text{Cl}_2\text{Cu}_2\text{N}_6\text{O}_4\cdot 4(\text{Cl})$ , F.W. = 916.97, 150 K,  $\lambda = 0.71073\text{ \AA}$ , monoclinic, space group C2/c,  $a = 28.01$  (4)  $\text{ \AA}$ ,  $b = 22.53$  (3)  $\text{ \AA}$ ,  $c = 14.76$  (2)  $\text{ \AA}$ ,  $\beta = 102.25$  (4)°,  $V = 9099$  (23)  $\text{ \AA}^3$ ,  $Z = 8$ ,  $D_c = 1.339\text{ Mg}\cdot\text{m}^{-3}$ ,  $\mu = 0.88\text{ mm}^{-1}$ ,  $F(000) = 3752$ , crystal dimensions:  $0.32 \times 0.22 \times 0.14\text{ mm}$ , Independent reflections: 8684 ( $R_{\text{int}} = 0.084$ ). The final anisotropic full-matrix least-squares refinement on  $F^2$  with 497 variables converged at  $R_1 = 0.14$ , for the observed data and  $wR_2 = 0.373$  for all data. Crystal data and structural refinement details are shown in Table S4 Additional crystallographic information, including bond distances and angles are shown in Tables S5–S8.

### 2.4. Enzyme activity determinations

The activities of acetylcholinesterase (AChE) from *Electrophorus*

**Table 1**  
Analytical and physical data for **HLa–e** and their  $\text{Cu}^{2+}$  complexes  $[\text{Cu}_2(\text{N}^{\text{H}}\text{La–e})_4]\text{Cl}_4$ .

Compound	Color	Yield (%)	m.p. (°C)	Minimum molecular formula	Found (Calc.) (%)		
					C	H	N
<b>HLa</b>	Yellow	72	208	$\text{C}_{18}\text{H}_{16}\text{ClN}_3\text{O}$	66.19 (66.36)	4.95 (4.95)	12.76 (12.90)
$[\text{Cu}_2(\text{N}^{\text{H}}\text{La})_4]\text{Cl}_4$	Green	69	242	$\text{C}_{36}\text{H}_{32}\text{Cl}_4\text{CuN}_6\text{O}_2 \cdot 2\text{H}_2\text{O}$	52.88 (52.60)	4.26 (4.41)	10.17 (10.22)
<b>HLb</b>	Yellow	79	240	$\text{C}_{18}\text{H}_{15}\text{BrClN}_3\text{O}$	53.42 (53.42)	3.74 (3.74)	10.14 (10.38)
$[\text{Cu}_2(\text{N}^{\text{H}}\text{Lb})_4]\text{Cl}_4$	Green	42	217	$\text{C}_{36}\text{H}_{30}\text{Br}_2\text{Cl}_4\text{CuN}_6\text{O}_2 \cdot 2\text{H}_2\text{O}$	44.32 (44.13)	3.63 (3.50)	8.52 (8.58)
<b>HLc</b>	Yellow	77	265	$\text{C}_{18}\text{H}_{15}\text{ClN}_4\text{O}_3$	58.34 (58.31)	4.09 (4.08)	15.06 (15.11)
$[\text{Cu}_2(\text{N}^{\text{H}}\text{Lc})_4]\text{Cl}_4$	Green	48	264	$\text{C}_{36}\text{H}_{30}\text{Cl}_4\text{CuN}_8\text{O}_6 \cdot 3\text{H}_2\text{O}$	46.87 (46.49)	3.75 (3.90)	12.22 (12.05)
<b>HLd</b>	Beige	75	158	$\text{C}_{19}\text{H}_{18}\text{ClN}_3\text{O}_2$	64.01 (64.13)	4.90 (5.10)	11.64 (11.81)
$[\text{Cu}_2(\text{N}^{\text{H}}\text{Ld})_4]\text{Cl}_4$	Green	41	208	$\text{C}_{38}\text{H}_{36}\text{Cl}_4\text{CuN}_8\text{O}_4 \cdot 2.5\text{H}_2\text{O}$	51.09 (51.22)	4.24 (4.64)	9.29 (9.43)
<b>HLe</b>	Yellow	81	176	$\text{C}_{19}\text{H}_{18}\text{ClN}_3\text{O}$	67.20 (67.15)	5.14 (5.34)	12.37 (12.37)
$[\text{Cu}_2(\text{N}^{\text{H}}\text{Le})_4]\text{Cl}_4$	Green	27	241	$\text{C}_{38}\text{H}_{36}\text{Cl}_4\text{CuN}_6\text{O}_2$	56.35 (56.06)	4.69 (4.46)	10.68 (10.32)

electricus and butyrylcholinesterase (BChE) from equine serum were monitored spectrophotometrically (Vmax Microplate reader; Molecular Device) at 405 nm by modified [34] Ellman's assay [35]. AChE stock solution (stock A) ( $25 \text{ units} \cdot \text{mL}^{-1}$ ) was prepared in phosphate buffer (100 mM, pH 7.4). An aliquot of stock A was then diluted 50 times with phosphate buffer to give stock B. BChE solution ( $2 \text{ units} \cdot \text{mL}^{-1}$ ) was diluted in phosphate buffer. Solutions of acetylthiocholine iodide (ATCI, 20 mM) and butyrylthiocholine iodide (BTCl, 40 mM) were prepared in distilled water. Ellman's reagent DTNB (5,5-dithio-bis-(2-nitrobenzoic acid)) (10 mM) was prepared in phosphate buffer (100 mM, pH 7.4). The samples were dissolved in DMSO at a concentration of 100 mM and diluted appropriately in phosphate buffer (100 mM, pH 7.4) to the desired concentrations immediately before use. All solutions were kept on ice during the experiment. The maximum DMSO concentration in the assay medium was 0.1% and did not inhibit the enzyme activity. All experiments were performed at  $25 \pm 1^\circ\text{C}$ . The values depicted in the tables are the average of two curves from assays performed in triplicate in a 96-wells plate.

### 2.5. In vitro inhibition of AChE

All experimental wells received AChE stock B ( $0.012 \text{ units} \cdot \text{mL}^{-1}$ ) or BChE ( $0.05 \text{ units} \cdot \text{mL}^{-1}$ ), DTNB (0.25 mM) and phosphate buffer (control – enzyme activity), or sample solutions (1 to 100  $\mu\text{M}$ ). The mixtures were incubated for 10 min at  $25^\circ\text{C}$ . ATCI (0.5 mM) or BTCl (1 mM) was then added to all wells and the plate was read immediately. The spontaneous hydrolysis of the substrate was evaluated by replacing enzyme for buffer. Inhibition is given relative to the control. All concentrations refer to final concentrations. The volume of the sample in each well was 0.2 mL.

### 2.6. $\text{Cu}^{2+}$ binding affinity

For the UV–Vis titrations, 2 mM stock solutions of **HLd** and  $\text{CuCl}_2 \cdot 2\text{H}_2\text{O}$  were prepared in DMSO because **HLd** and the product are insoluble in water. The measurements were made in 0.1 M solutions of HEPES buffer at pH 6.6 and 7.4. In agreement with the limits of the Beer–Lambert law ( $A = b \cdot c \cdot \epsilon$ , with  $A < 1$ ) the concentration selected for **HLd** was about  $48 \mu\text{M}$ , i.e.  $50 \mu\text{L}$  of the **HLd** stock solution were added to 2 mL of the buffer solutions. Increasing amounts of the  $\text{CuCl}_2 \cdot 2\text{H}_2\text{O}$  stock solution were added to the **HLd** containing HEPES solutions (1:0.25; 1:0.5; 1:0.75; 1:1, 1:1.25; 1:1.5 – **HLd**: $\text{Cu}^{2+}$  stoichiometry). The solutions were thoroughly mixed and the spectra, recorded after incubating for 3 min, at room temperature.

### 2.7. Mixed brain cultures

Primary mixed brain cultures were prepared as previously described [36] from the cerebral cortex of newborn mice. Briefly, single cell suspensions were obtained by dissociating cells from the cerebral cortex

in Dulbecco's modified Eagle medium (DMEM)/F12 supplemented with glucose (33 mM), glutamine (2 mM), sodium bicarbonate (3 mM), penicillin/streptomycin ( $0.5 \text{ mg} \cdot \text{mL}^{-1}$ ), fungizone ( $2.5 \text{ g} \cdot \text{mL}^{-1}$ ) and fetal bovine serum 10% (FBS, v/v). The cells were plated on pre-coated poly-L-lysine ( $5 \mu\text{g} \cdot \text{mL}^{-1}$ ) plates and grown in a DMEM/F12 enriched medium with 10% FBS. The cultures were incubated at  $37^\circ\text{C}$  in a humidified 5%  $\text{CO}_2$  and 95% air atmosphere. The medium was changed 5 days after seeding and assays were performed 7 days after culture preparation.

### 2.8. 3-(4,5-Dimethylthiazol-2-yl)-2,5-diphenyltetrazolium bromide (MTT) cytotoxicity assays

For the MTT analysis, cells were plated on a 96-well plate. Mixed brain cultures were washed three times with serum-free DMEM/F12 medium and treated with **HLa** (55–50  $\mu\text{M}$ ), **HLb** (7.5–75  $\mu\text{M}$ ), **HLc** (9.5–95  $\mu\text{M}$ ), **HLd** (9.5–95  $\mu\text{M}$ ), **HLe** (7.5–75  $\mu\text{M}$ ), tacrine (0.045–45  $\mu\text{M}$ ) or  $[\text{Cu}_2(\text{N}^{\text{H}}\text{Ld})_4]\text{Cl}_4$  (2.8–27.5  $\mu\text{M}$ , i.e.  $[\text{Cu}(\text{N}^{\text{H}}\text{Ld})_2]\text{Cl}_2$  5.5–55  $\mu\text{M}$ ) in serum-free DMEM/F12 for 24 or 48 h. The concentrations used in the assays were based on the AChE inhibitory  $\text{IC}_{50}$  values obtained for these compounds. Viable cells were quantified by the MTT cytotoxicity assay as previously described [37]. The cell survival fraction was measured at each drug concentration as the ratio of absorbance at 560 nm, relative to vehicle-treated cells.

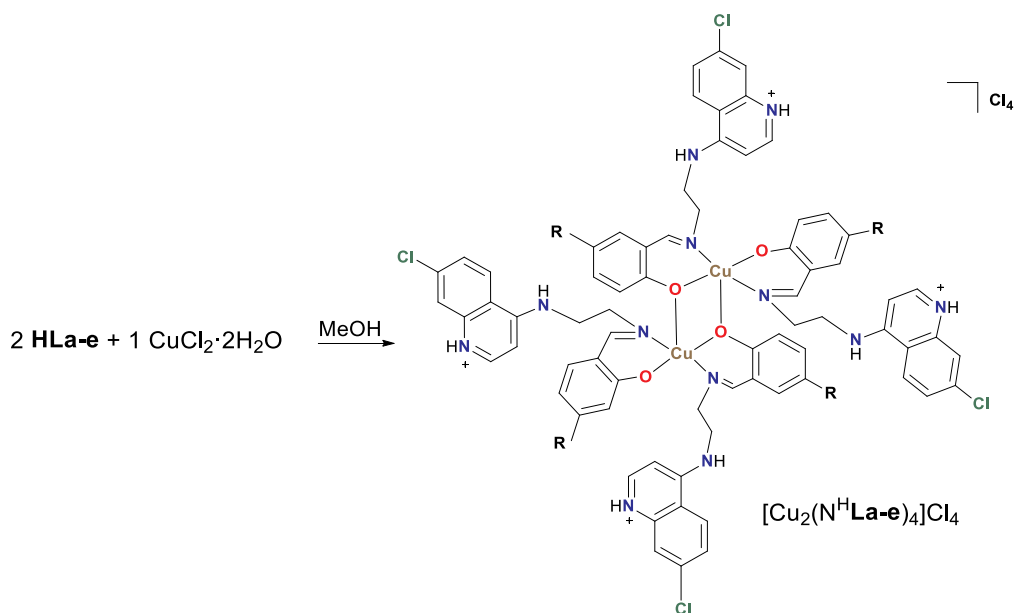
### 2.9. Immunocytochemistry

Cells were plated on coverslips placed on a 24-well plate. The procedure was performed as described in the literature [38]. Briefly, cells were fixed with 4% paraformaldehyde in phosphate buffer for 10 min and incubated with 5% bovine serum albumin (BSA) diluted in PBS for 30 min. The cells were then incubated overnight at  $4^\circ\text{C}$  with an Anti- $\beta$  III Tubulin mAb antibody (Promega; # G712) and a Polyclonal Rabbit Anti-Glial Fibrillary Acidic Protein antibody (GFAP, Dako, # Z 0334), followed by incubation with secondary antibodies conjugated with Alexa Fluor® 488 or Alexa Fluor® 546 for 1 h. Then, the cells were stained with DAPI and mounted. The cells were imaged using an epifluorescence Nikon microscope (TE300). Image processing was done using Adobe Photoshop®.

### 2.10. Statistical analysis

The data were analyzed by One-Way ANOVA followed by *post hoc* comparisons (Dunnett's test).

For the enzyme tests the absorbance/min values were calculated with the software Softmax Pro 6.4. Inhibition values were calculated through non-linear regression with the software GraphPadPrism 5 (GraphPad software®, San Diego, CA, USA). For each sample, results correspond to average  $\pm$  standard deviation of two experiments, each one, performed in triplicate.



**Scheme 1.** Synthesis of the copper complexes  $[\text{Cu}_2(\text{N}^{\text{H}}\text{La-e})_4]\text{Cl}_4$ .

## 2.11. Molecular modeling studies

### 2.11.1. Molecular docking

Docking calculations were carried out to obtain the starting poses of ligands **HLa-e**, for the molecular dynamics (MD) simulations, and to make a comparison of the binding modes of these ligands to the known AChE inhibitor donepezil. Also, two possible monomeric solution forms of the **HLd**  $\text{Cu}^{2+}$  complexes ( $[\text{Cu}(\text{N}^{\text{H}}\text{Ld})_2]^{2+}$  and  $[\text{Cu}(\text{N}^{\text{H}}\text{Ld})(\text{Ld})]^+$ ) were docked inside *EeAChE* in order to evaluate the affinities of these species for AChE. To prepare the ligands and complexes for docking, all hydrogen atoms were added and Gasteiger charges were assigned. The AutoDockTools (ADT) [39] was used to merge nonpolar hydrogens and define which bonds were rotatable. These compounds were docked inside the crystallographic structure of AChE from *Electrophorus electricus* (*EeAChE*), available in the proteins data bank (PDB) (<http://www.rcsb.org/pdb/home/home.do>) under the code 1C2B, by using a Lamarckian genetic algorithm search. Each compound was docked in 100 trials with 100 orientations per trial and the binding site centered in the gorge of the active site of *EeAChE*. The highest affinity orientation was selected after 500,000 energy evaluations. The parameters for the genetic algorithm followed the default parameters of the AutoDock program [39]. After 100 docking runs, the obtained orientations were analyzed. The orientation of each compound with the lowest docking-energy was considered as the most stable conformation.

No experimental structure of *EeAChE* complexed with an inhibitor is available in the PDB (<http://www.rcsb.org/pdb/home/home.do>), therefore the docking protocol used was validated through the redocking of donepezil over itself in the crystallographic structure of human (*Homo sapiens sapiens*) AChE (*HsAChE*) complexed with donepezil, available in the PDB under the code 4EY7.

### 2.11.2. Molecular dynamics

The GROMACS 5.0.4 package with the Gromos96/53a6 force field was used for the MD simulations [40]. Ligands **HLa-e** were parameterized in the Gromos96/53a6 force field using the ATB site [41]. All *EeAChE*-ligand complexes were simulated in a dodecahedron box with a solute-wall distance of 1.2 nm, SPC water model and balanced with  $\text{Na}^+$  counter ions. Previous to the 20 ns of MD production, the following steps were followed: i) energy minimization with the Steepest Descent algorithm until a maximum force  $< 41.84 \text{ kcal}\cdot\text{mol}^{-1}$ ; ii) 100 ps of NVT equilibration in order to equilibrate the pressure, with

positions restraints (PR) of enzyme and ligand, leap-frog integrator and V-rescale thermostat [42]; iii) 100 ps of NPT equilibration in order to equilibrate volume, with PR of the protein and ligand, leap-frog integrator, V-rescale thermostat and  $T = 310 \text{ K}$ . In each cycle a convergence energy criterion of  $4.184 \times 10^{-6} \text{ kcal}\cdot\text{mol}^{-1}$  was used between successive steps. Finally the MD simulations (20 ns) of production in an NPT ensemble (fixed number of atoms, constant pressure, and temperature) were performed with the following considerations: MD at physiological temperature of 310 K without any restriction, using 2 fs of integration time and saved data at each 2 ps, PME (particle Mesh Ewald) [43] for the long range electrostatic interactions, with a cut-off = 1.4 nm, V-rescale algorithm for the temperature coupling (thermostat) and Parrinello-Rahman barostat for the pressure coupling. Van der Waals interactions were considered up to a cut-off of 1 nm [44].

## 3. Results and discussion

### 3.1. Synthesis of the Schiff bases and copper complexes

The 7-chloroquinoline Schiff bases **HLa** [22], **HLb-HLd** [23] and **HLe** were synthesized (72–81%) by treatment of the  $\text{N}^1$ -(7-chloroquinolin-4-yl)ethane-1,2-diamine precursor with excess of various salicylaldehydes in refluxing or heating in EtOH, and their identity and purity were confirmed by elemental analysis, melting point, IR and  $^1\text{H}$  and  $^{13}\text{C}$  NMR spectroscopy (Tables 1 and S2 and Figs. S1–S20). All compounds are insoluble in water, soluble in DMSO and sparingly soluble in MeOH.

The copper complexes were obtained from the reactions of  $\text{CuCl}_2 \cdot 2\text{H}_2\text{O}$  with **HLa-e** in a 1:2 (copper to ligand) molar ratio in MeOH (Scheme 1). The products  $[\text{Cu}_2(\text{N}^{\text{H}}\text{La-e})_4]\text{Cl}_4$  were isolated in 27–69% yields in the form of green powders. They are all insoluble in water, but very soluble in DMSO, whereas  $[\text{Cu}_2(\text{N}^{\text{H}}\text{Ld})_4]\text{Cl}_4$  is moderately soluble in MeOH. Elemental analyses confirmed a 1:2:2 metal to ligand to chloride stoichiometry (Table 1). The dinuclear nature of all complexes in the solid state was established by EPR studies, which also evidenced formation of mononuclear species in DMSO. An X-ray diffraction study of  $[\text{Cu}_2(\text{N}^{\text{H}}\text{Ld})_4]\text{Cl}_4$  corroborated the solid state EPR results and confirmed the formation of the dinuclear compounds in which each metal ion is coordinated by two protonated ligand molecules.

### 3.2. IR spectroscopy

The band around  $3400\text{ cm}^{-1}$ , attributed to the free phenolic OH group (**HLa**, **HLd** and **HLe**), is absent in the spectra of the complexes (see Figs. S21–S25 and Table S1), whereas the  $\nu(\text{C}=\text{O})$  stretching band, around  $1280\text{ cm}^{-1}$  in the spectra of all the free ligands, is shifted to around  $1300\text{ cm}^{-1}$ , thus indicating formation of the Cu–O bond *via* deprotonation [45]. Changes were also observed in the  $1640\text{--}1550\text{ cm}^{-1}$  region of the spectra of all ligands upon coordination. The medium intensity band around  $1635\text{ cm}^{-1}$ , attributed to the imine  $\nu(\text{C}=\text{N})$ , is shifted to lower wavenumber in the spectra of the complexes confirming coordination *via* the imine nitrogen [46]. These data clearly indicate that the ligand coordinates to the metal *via* the imine-phenolate portion. A band associated with the  $\nu\text{C}=\text{N}$  of the 7-chloroquinoline nucleus at  $1581\text{--}1572\text{ cm}^{-1}$  in the spectra of **HLa–e** is shifted in those of compounds  $[\text{Cu}_2(\text{N}^{\text{H}}\text{La–e})_4]\text{Cl}_4$ . This could be due to protonation of the coordinated ligand (referred to as  $\text{N}^{\text{H}}\text{La–e}$ ) either at the amine nitrogen [47], or at the 7-chloroquinoline nitrogen. The second proposal is supported by an X-ray diffraction study of  $[\text{Cu}_2(\text{N}^{\text{H}}\text{Ld})_4]\text{Cl}_4$  described below, and also by  $\text{pK}_a$  values (the acid dissociation constant of the quinolinium cation) from the literature for compounds with the same 7-chloroquinoline core as **HLa–e** (e.g.  $N^1, N^1$ -diethyl- $N^2$ -(7-chloro-4-quinolinyl)-1,2-ethanediamine), which confirm the higher basicity of the 7-chloroquinoline nitrogen ( $\text{pK}_a = 7.56$ ) compared with that of the amine nitrogen [48].

### 3.3. Crystal structure analysis of $[\text{Cu}_2(\text{N}^{\text{H}}\text{Ld})_4]\text{Cl}_4$

The compound crystallizes in the monoclinic space group  $\text{C}2/c$  and its symmetric unit consists of a tetracationic centrosymmetric *bis*( $\mu$ -phenoxo)di-copper(II) complex neutralized by four non coordinated chloride ions, thus confirming that the ligands are protonated. The binuclear unit exhibits two penta-coordinated copper centers in a

distorted square pyramidal geometry ( $\tau = 0.24$ ) [49] (Fig. 2A) with the coordination sphere formed by two phenol-deprotonated Schiff base ligands acting as bidentate *N,O* chelates, one of which also acts as a  $\mu$ -bridging ligand to the other copper atom, similar to other *N*-alkyl-salicylideneiminato copper complexes reported earlier [45,50–52]. The basal plane is constituted by two imine nitrogen atoms, one phenolate oxygen and one bridging phenolate oxygen atoms, whereas the apical site is occupied by another bridging phenolate oxygen atom that is basal to the second copper ion of the dimer. The imine nitrogen to the central metal atom bond distances (Cu(1)–N(3), 2.022(8) and Cu(1)–N(6) 2.009(8) Å) are in the typical range for penta-coordinated  $\text{Cu}^{2+}$  complexes (1.993(9)–2.025(9) Å). The Cu(1)–O(1) axial bond length (2.390(7) Å) is longer than the equatorial distances (1.909(7) Å) as observed in similar binuclear complexes. The intramolecular non-bonding Cu(1)⋯Cu(1') distance, 3.262 Å, is shorter than those observed for other similar  $\text{Cu}^{2+}$  binuclear systems, probably as the result of  $\pi$ – $\pi$  stacking interactions between the phenyl rings and between the quinoline rings, which stabilize the binuclear arrangement. Important features of the structure are the C(11)–N(2)–C(4) angle of  $124.6(9)^\circ$ , indicative of the amine nitrogen electron pair delocalization over the quinoline nucleus, and the  $\text{N}^+(1)\text{--H}\cdots\text{Cl}^-$  interaction, which confirm that N(1) is the site of the ligand protonation (Fig. 2B).

### 3.4. UV–Vis spectra

The solution UV–Vis absorption spectra of **HLa–e** and complexes  $[\text{Cu}_2(\text{N}^{\text{H}}\text{La–e})_4]\text{Cl}_4$  were measured in DMSO due to low solubility in other solvents (Table S2 and Figs. S26–S30). The intense high-energy band at 330–340 nm ( $\epsilon = 1.3\text{--}1.8 \times 10^4\text{ M}^{-1}\text{cm}^{-1}$ ) in the spectra of the ligands and complexes are associated with aromatic  $\pi$ – $\pi$  intraligand charge-transfer. Upon coordination, the band at 410–440 nm ( $\epsilon = 7.8 \times 10^4\text{--}4.3 \times 10^5\text{ M}^{-1}\text{cm}^{-1}$ ) in the spectra of **HLa–e**, assigned to the  $n\text{--}\pi^*$  transition of the imine group, is blue shifted to 380 nm

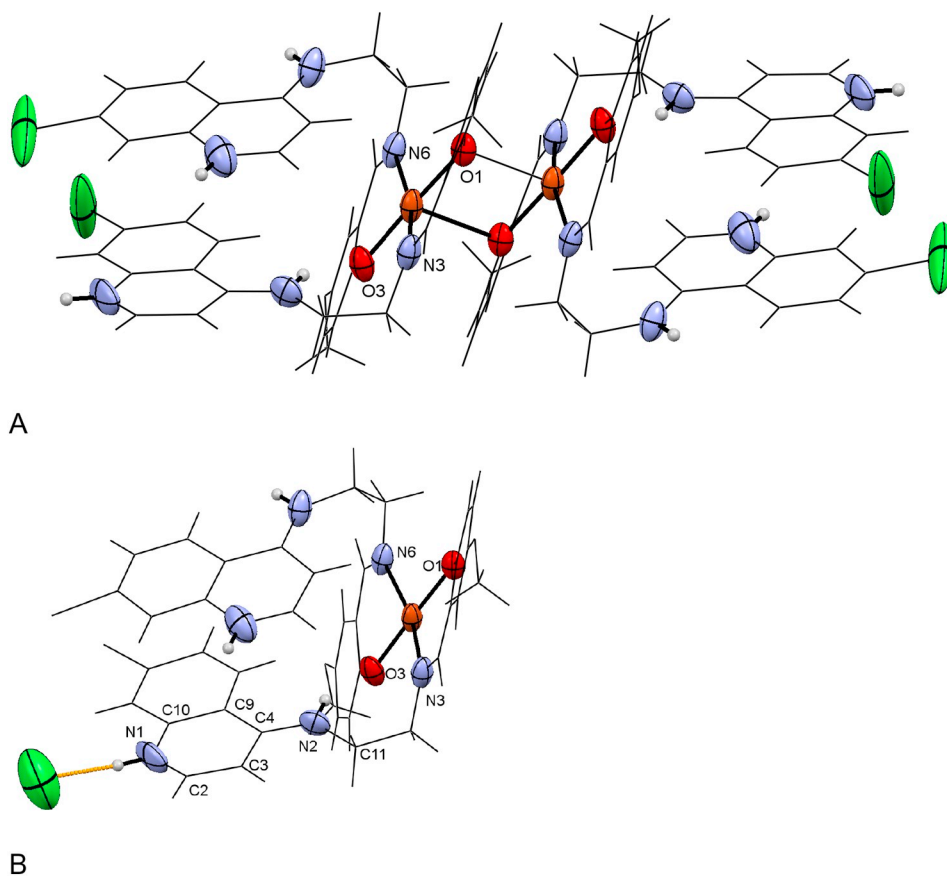


**Fig. 2.** A) Molecular geometry and atomic labeling scheme used in the description of  $[\text{Cu}_2(\text{N}^{\text{H}}\text{Ld})_4]\text{Cl}_4$ . Chloride ions and most hydrogen atoms have been omitted for clarity. Only selected atoms of the asymmetric unit are labeled. Atom ellipsoids are drawn at 50% of probability levels. Interatomic distances and angles are listed in Table S6 of the Supplementary information. B) Asymmetric unit with the labeling of the metal coordination sphere, the aminequinolinium unit and the  $\text{N}^+(1)\text{--H}\cdots\text{Cl}^-$  interaction.

( $\epsilon = 4.3\text{--}9.3 \times 10^3 \text{ M}^{-1}\text{cm}^{-1}$ ). A very broad, low intensity band in the visible region of the spectra of concentrated solutions of  $[\text{Cu}_2(\text{N}^{\text{H}}\text{La-e})_4]\text{Cl}_4$  is attributed to *d-d* transitions [53].

### 3.5. EPR spectra

X-band EPR spectra of the complexes are shown in Figs. S31A–S35A. Powder samples were analyzed at both 77 K and room temperature and resulted in characteristic axial spectra, with prominent parallel and perpendicular *g*-tensor features for all samples, along with a clear and pronounced Half Field Transition (HFT), confirming a  $S = 1$  magnetic binuclear system, in accordance with the solid state structure of  $[\text{Cu}_2(\text{N}^{\text{H}}\text{La-e})_4]\text{Cl}_4$ . Spectral simulations further confirmed the axiality of the gyromagnetic tensors corresponding to an elongation of a ligand axis and consequent stabilization of the copper  $3dx^2-y^2$  orbital. This situation can lead to various distorted penta- and hexa-coordinated axial geometries for the copper center. However, one exception was found for sample  $[\text{Cu}_2(\text{N}^{\text{H}}\text{Ld})_4]\text{Cl}_4$ , which presented a rhombic *g*-tensor in an indication of dynamic Jahn-Teller effect.

The solution spectra of all complexes, obtained in frozen DMSO (due to low solubility in other solvents), are typical of mononuclear  $\text{Cu}^{2+}$  complexes. They contain two mononuclear components identified by spectral simulation (Table S3 and Figs. S31B–35B) and no HFT signal, thus indicating that the dinuclear structure is destroyed in solution, via cleavage of the elongated Cu–O1 bond (Fig. 2) and replacement of the alkoxide oxygen by a DMSO molecule. Dissociation of analogous dimeric *N*-alkyl-salicylideneaminato copper complexes in pure toluene and toluene solutions containing polar solvents, such as pyridine, DMF and DMSO, has been previously reported [54–56].

Spectral simulations pointed to two species found in all samples that have the same spectral origin, i.e., from the geometrical point of view, the copper center in all samples contains the same ligands and geometry in both species. We attributed these components to two distinct elongated Jahn-Teller conformations of the same structure, one with average  $g_{\parallel} = g_z = 2.4080$ ,  $g_x = g_y = g_{\perp} = 2.0764$ ,  $A_z = A_{\parallel} = 376.8 \text{ MHz}$  (species 1), and the other with average  $g_{\parallel} = g_z = 2.3749$ ,  $g_x = g_y = g_{\perp} = 2.0819$ ,  $A_z = A_{\parallel} = 432.2 \text{ MHz}$  (species 2). Species 1 population is slightly higher (57% total) than species 2. The structural difference between species 1 and 2 is that in the former the relation  $A_{\parallel}/g_{\parallel}$  correlates unequivocally to an equatorial coordination of four oxygen atoms (4O), and in the later the relation can be assigned to a coordination of three oxygen atoms and one nitrogen atom (1N3O) (Scheme 2) [57]. Presumably the additional oxygen donors originate from the DMSO solvent molecules.

### 3.6. Molar conductance and mass spectra

In order to further investigate the nature of these species in solution the molar conductance of compounds  $[\text{Cu}_2(\text{N}^{\text{H}}\text{La-e})_4]\text{Cl}_4$  was measured in dry DMSO at 1 mM solution (Table S2). The values were found to be in the range of 31.8–43.2 ( $\Omega^{-1}\text{cm}^2\text{mol}^{-1}$ ) corresponding to two ions in solution, suggesting that the species are 1:1 electrolytes, instead of the expected 1:2 [58]. According to the EPR solution spectra (*vide supra*), the dimers are cleaved in DMSO and the resulting species, solvated (see Scheme 2). It is possible that water present in the sample (see Table 1) or/and in the solvent is responsible for partial deprotonation of the ligand, resulting in species of the type  $[\text{Cu}(\text{N}^{\text{H}}\text{La-e})(\text{La-e})](\text{DMSO})\text{Cl}$ , which may well be one of the species observed in the EPR solution spectra.

The ESI-MS of the metal complexes  $[\text{Cu}_2(\text{N}^{\text{H}}\text{La-e})_4]\text{Cl}_4$  dissolved in DMSO and diluted in MeOH support this proposal (Figs. S36–S41). They all show peaks indicative of the formation of the monovalent  $[\text{Cu}(\text{N}^{\text{H}}\text{La-e})(\text{La-e})]^+$  and divalent  $[\text{Cu}(\text{N}^{\text{H}}\text{La-e})_2]^{2+}$  species. The experimental spectrum together with the simulated isotopic distribution of the  $[\text{Cu}(\text{N}^{\text{H}}\text{Ld})(\text{Ld})]^+$  species ( $m/z^+ = 772$ ) derived from  $[\text{Cu}_2(\text{N}^{\text{H}}\text{Ld})_4]\text{Cl}_4$  are shown in Fig. 3.

### 3.7. Cholinesterases inhibitory activities

The inhibitory activity of **HLa-e** and metal compounds  $[\text{Cu}_2(\text{N}^{\text{H}}\text{La-e})_4]\text{Cl}_4$  (which in solution are monomers) was evaluated using a modification of Ellman's spectrophotometric method in AChE from electric eel and BChE from equine serum, to investigate the selectivity of the tested compounds. Because the compounds were insoluble in water, they were first dissolved in DMSO, followed by dilution in phosphate buffer (pH 7.4) to the desired concentrations, with a maximum concentration of DMSO of 0.1%.

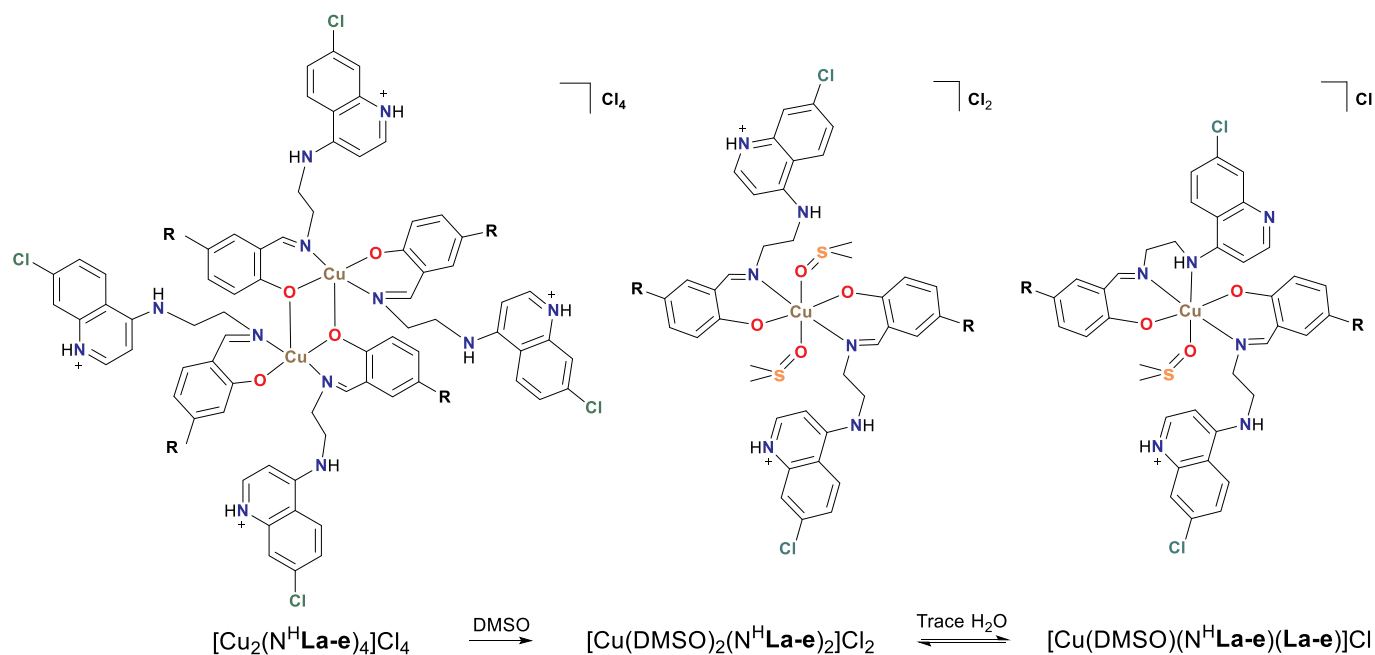
Except for the copper complex of **HLe** the compounds inhibited AChE in a concentration-dependent manner. In comparison with tacrine ( $\text{IC}_{50} = 0.041 \pm 0.0002 \mu\text{M}$ ), however, all compounds were much less active (Table 2). They showed selectivity for AChE as none inhibited BChE. In general **HLa-e** were better inhibitors than their copper complexes, except for the mononuclear complex derived from  $[\text{Cu}_2(\text{N}^{\text{H}}\text{Ld})_4]\text{Cl}_4$  ( $\text{IC}_{50} = 5.45 \pm 0.70 \mu\text{M}$ ) that inhibited AChE more efficiently than **HLe** ( $\text{IC}_{50} = 9.31 \pm 1.17 \mu\text{M}$ ). This result might be related to the higher solubility of this complex in a hydrogen donor solvent (MeOH), and thus possibly in the 0.1% DMSO/phosphate buffer), compared to the other complexes, which were only soluble in DMSO (see Section 3.1). One may speculate that in the AD affected brain **HLe** may compete for the loosely bound  $\text{Cu}^{2+}$  and form a complex, which in turn would inhibit AChE. Therefore, **HLe** could act in a bifunctional manner, by reducing metal-induced A $\beta$  aggregation, oxidative stress and therefore neurotoxicity, in addition to inhibiting AChE. Reports in the literature on the cholinesterase inhibitory activity of  $\text{Cu}^{2+}$  complexes and especially on the improvement of the activity of the proligands upon coordination to  $\text{Cu}^{2+}$  are rare [59,60]. Investigation of the cholinesterase activities of an iminoquinoline Schiff base **HL'** obtained from the reaction of salicylaldehyde with 2-aminoquinoline, thus related to **HLa-e** (*N,O*-chelates), and its metal complexes ( $\text{ML}'_2$ ), revealed that the  $\text{Cu}^{2+}$  and  $\text{Co}^{2+}$  complexes (but not the  $\text{Zn}^{2+}$  and  $\text{Ni}^{2+}$  ones) selectively inhibited BChE ( $\text{IC}_{50} (\mu\text{M}) \pm \text{SEM} = 69 \pm 0.0112$  and  $5 \pm 0.0004$ , respectively), whereas the free ligand **HL'** showed no activity at all.

### 3.8. The chelating effect of **HLe** toward $\text{Cu}^{2+}$ ions

The ability of imine **HLe** to chelate  $\text{Cu}^{2+}$  ions under acidosis conditions (pH 6.6) and in physiological (pH 7.4), in HEPES buffers, was investigated by spectrophotometric titrations. The UV-Vis spectra of a solution of **HLe**, which was dissolved in DMSO and diluted in HEPES (pH 6.6), titrated with aliquots of  $\text{Cu}^{2+}$  is shown in Fig. 4. In the absence of  $\text{Cu}^{2+}$ , the UV-Vis spectrum of the ligand showed the aromatic  $\pi$ - $\pi$  intraligand charge-transfer absorption bands at 330–340 nm and the band at 435 nm attributed to the  $n$ - $\pi^*$  transition of the imine group. Upon increasing the concentration of  $\text{Cu}^{2+}$  the intensity of the later absorption band decreased, and a new band around 380 nm appeared, which was associated with the copper complex formation (see Section 3.4). The stoichiometry of this reaction was investigated by following the absorption changes at 380 nm. The results showed that the absorbance linearly increased initially and then plateaued, being consistent with a 1:2  $\text{Cu}^{2+}$ :ligand molar ratio (Fig. 4 inset and Fig. S42 – Job's plot). Indeed, the final spectrum is exactly the same as that of the monomer formed when  $[\text{Cu}_2(\text{N}^{\text{H}}\text{Ld})_4]\text{Cl}_4$  is dissolved in the same amounts of DMSO/HEPES (pH 6.6) (Fig. S43). Similar behavior was observed for the spectrophotometric titrations carried out at pH 7.4 (Fig. S44), except that the band associated with the formation of the complex is broader and shifted to around 400 nm, possibly due to the formation of species resulting from ligand deprotonation.

### 3.9. Pharmacokinetic properties of compounds **HLa-e**

The following parameters associated with solubility and permeability were calculated for **HLa-e** and are gathered in Table 3: the



Scheme 2. Proposed structures for the copper species 1 and 2 in DMSO.

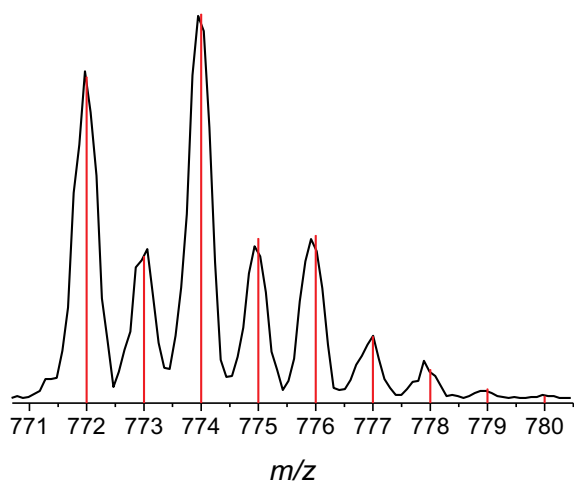
Fig. 3. Isotopic distribution for  $[\text{Cu}(\text{N}^{\text{H}}\text{Ld})(\text{Ld})]^+$  derived from  $[\text{Cu}_2(\text{N}^{\text{H}}\text{Ld})_4]^{4+}$ . Simulated data: vertical lines; experimental spectrum: continuous line.

Table 2

IC<sub>50</sub> values of *Ee*AChE inhibition for **HLa–e** and their monomer metal complexes.

Ligand	IC <sub>50</sub> (μM)	Complex	IC <sub>50</sub> (μM)
<b>HLa</b>	4.61 ± 0.48	$[\text{Cu}(\text{N}^{\text{H}}\text{La})_2]\text{Cl}_2$	41.28 ± 3.15
<b>HLb</b>	7.17 ± 0.43	$[\text{Cu}(\text{N}^{\text{H}}\text{Lb})_2]\text{Cl}_2$	44.16 ± 2.50
<b>HLc</b>	9.23 ± 0.36	$[\text{Cu}(\text{N}^{\text{H}}\text{Lc})_2]\text{Cl}_2$	> 100
<b>HLd</b>	9.31 ± 1.17	$[\text{Cu}(\text{N}^{\text{H}}\text{Ld})_2]\text{Cl}_2$	5.45 ± 0.70
<b>HLe</b>	7.34 ± 0.06	$[\text{Cu}(\text{N}^{\text{H}}\text{Le})_2]\text{Cl}_2$	64.67 ± 2.20
		Tacrine	0.041 ± 0.0002
		Donepezil <sup>a</sup>	0.051 ± 0.004

<sup>a</sup> From ref. [61].

theoretical octanol/water partition coefficients (Clog P), molecular weight (MW), the number of H-bond donors (HBD – expressed as the sum of OHs and NHs) and the number of acceptors (HBA – the sum of Ns and Os). Lipinski's rule of five, used to predict the suitability of orally

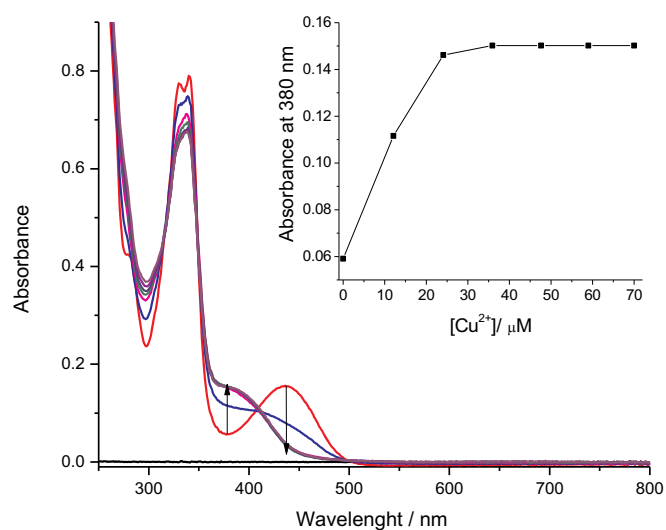


Fig. 4. Spectral changes of **HLd** (48 μM) in a HEPES buffer solution (0.1 M, pH 6.6) upon addition of aliquots of a 2 mM solution of  $\text{CuCl}_2 \cdot 2\text{H}_2\text{O}$  in DMSO/HEPES pH = 6.6: — **HLd**, — **HLd** +  $\text{Cu}^{2+}$  (12.5 μL), — **HLd** +  $\text{Cu}^{2+}$  (25 μL), until — **HLd** +  $\text{Cu}^{2+}$  (75 μL). Inset: change in the absorbance at 380 nm with increased concentration of  $\text{Cu}^{2+}$  derived from the UV–Vis titration, consistent with a 2:1 ligand to metal molar ratio.

Table 3

Molecular descriptors of compounds **HLa–e** and tacrine.

Compounds	Clog P	MW	HBD	HBA
<b>HLa</b> (R = H)	4.49	325.80	2	2
<b>HLb</b> (R = Br)	5.46	404.69	2	2
<b>HLc</b> (R = NO <sub>2</sub> )	4.46	370.79	2	2
<b>HLd</b> (R = OCH <sub>3</sub> )	4.60	355.82	2	2
<b>HLe</b> (R = CH <sub>3</sub> )	4.99	339.82	2	2
Tacrine	3.27	198.26	1	2

Clog P value was calculated using ChemDraw Ultra 13.0 [64].

administered drug candidates, states that poor absorption or permeation is expected when  $MW > 500$ ,  $HBD > 5$ ,  $HBA > 10$  or  $Clog P > 5$  [62]. For Central Nervous System (CNS) penetration, the drugs physical properties have a smaller range than general therapeutics, CNS penetration being likely if  $MW < 400$ ,  $HBD \leq 3$ ,  $HBA \leq 7$  and  $Clog P \leq 5$  [63]. The results indicate compounds **HLa**, **HLd** and **HLe** satisfy the criteria of the Lipinski's rule of 5 for CNS.

### 3.10. Neurotoxic effects

Primary mixed brain cultures were treated with different concentrations of **HLa–e**, tacrine and of the monomers of  $[Cu_2(N^H Ld)_4]Cl_4$  (which were defined based on their AChE inhibitory  $IC_{50}$  values). Cell viability was assessed after 24 and 48 h. The cells remained viable after treatment with all compounds at concentrations ranging from 0.045 to 0.45  $\mu M$ , including with the copper complex (Fig. S45, A–G), indicating that these compounds are not neurotoxic and should be good candidates as drugs in the AD treatment. Neurons and astrocytes were identified by immunostaining using the  $\beta$ -Tubulin III and GFAP antibodies, respectively, attesting the efficiency of the mixed brain culture method (Fig. S46).

### 3.11. Molecular modeling

#### 3.11.1. Docking studies

The best re-docking result obtained for donepezil inside *HssAChE* (shown in Fig. S47) presented a Root Mean Square Deviation (RMSD) value for the superposition of the non-hydrogen atoms of 1.81 Å. According to the literature a RMSD value below 2.0 Å is considered acceptable [65], therefore these results validate the docking protocol used for the enzyme.

Table 4 presents the energy results and the residues contributing for the stabilization of the best poses of donepezil, ligands **HLa–e**, and the complexes  $[Cu(N^H Ld)_2]^{2+}$  and  $[Cu(N^H Ld)(Ld)]^+$ , inside *EeAChE*, during the docking calculations (Figs. 5 and 6).

As can be observed, all ligands presented close negative values of energy, with the best result observed for **HLa** ( $-9.55 \text{ kcal}\cdot\text{mol}^{-1}$ ) and the worse for **HLc** ( $-6.67 \text{ kcal}\cdot\text{mol}^{-1}$ ). These results fit quite well to the experimental results shown in Table 2. In comparison with donepezil, all ligands presented similar energy values. This suggests that they are also capable of binding to *EeAChE*. The negative values and the large number of stabilizing residues suggest that all compounds have a good affinity for the gorge of *EeAChE*. Also it is possible to see that all ligands docked with similar orientations, in the same pocket, between residues from the catalytic anionic site (CAS) (Glu202, Ser203 and His447) and the peripheral anionic site (PAS) (Tyr124, Trp286) of *EeAChE*, similarly to donepezil [66–68]. Particularly and in agreement with the experimental results (Table 2) complexes  $[Cu(N^H Ld)_2]^{2+}$  and  $[Cu(N^H Ld)(Ld)]^+$  presented better energy values (more negative) than all ligands, except for **HLa**, thus suggesting that these complexes can effectively bind to the active site of *EeAChE*.

**Table 4**

Docking results for the best poses of donepezil, compounds **HLa–e**, and the complexes  $[Cu(N^H Ld)_2]^{2+}$  and  $[Cu(N^H Ld)(Ld)]^+$ , inside *EeAChE*.

Molecules	Binding energies (kcal·mol <sup>-1</sup> )	Interacting residues
Donepezil	-7.90	Trp286, Leu289, Gln291, Ile294, Phe338, Tyr341
<b>HLa</b>	-9.55	Gly120, Gly121, Tyr124, Glu202, Ser203, Ser293, Ile294, Phe295, Phe297, Tyr337, Phe338, Tyr341, His447, Gly448.
<b>HLb</b>	-8.61	Trp86, Gly120, Gly121, Tyr124, Ser125, Ile294, Phe295, Phe338, Tyr341.
<b>HLc</b>	-6.67	Trp86, Gly121, Tyr124, Ser203, Trp286, Leu289, Ser293, Phe297, Tyr337, Phe338, Tyr341.
<b>HLd</b>	-7.92	Trp86, Gly120, Gly121, Tyr124, Ser203, Trp286, Phe297, Tyr337, His447.
<b>HLe</b>	-7.56	Trp86, Gly120, Gly121, Tyr124, Ser203, Trp286, Ile294, Phe295, Phe297, Tyr337, Phe338, His447.
$[Cu(N^H Ld)_2]^{2+}$	-8.90	Trp286, Ile294, Phe295, Phe297, Phe338, Tyr341, Gly342, Tyr377.
$[Cu(N^H Ld)(Ld)]^+$	-8.80	Tyr72, Thr75, Leu76, Trp286, Leu289, Glu292, Phe295, Phe295, Tyr341, Gly342.

#### 3.11.2. Molecular dynamics simulations

After the docking studies, the best poses of each ligand were submitted to 20.0 ns of MD simulations in order to verify their dynamic behavior and analyze the interactions observed inside the enzyme. Therefore studies of the variation of total energy and RMSD were performed. The plots of variation of total energy during the MD simulations for the 5 simulated systems (data not shown) point to stabilization after 10 ns of simulation, with an average energy around  $-2.80 \times 10^6 \text{ kcal}\cdot\text{mol}^{-1}$  for all systems, suggesting structural stabilization. The temporal RMSD calculations were performed on all atoms of each complex to 2500 frames at every 20 ps, during the 20.0 ns of simulation. Considering that the complexes could fluctuate in the box, each frame was adjusted by the least squares method to its previous one for the calculation of the standard deviation. As shown in Fig. 7, the systems achieve equilibrium around the initial 7000 ps of simulation with maximum deviations below 0.24 nm (2.4 Å) and 0.18 nm (1.8 Å) for the protein and ligand, respectively. These results suggest that the ligands accommodate well inside *EeAChE* during the 20.0 ns of simulation, showing stabilization of the system and confirming the results obtained from the total energy calculations previously described. Analysis of Fig. 7 shows that **HLa** was the ligand with the smallest fluctuation during the simulation time, stabilizing below 0.05 nm (0.5 Å), in clear contrast to the other ligands. This suggests a greater stabilization inside the enzyme and, therefore, more affinity, corroborating experimental data and the docking results described above.

## 4. Conclusions

The AChE inhibitory activity of a series of chelating molecules derived from 1,2-ethanediamine, *N*<sup>1</sup>-(7-chloro-4-quinolinyl) and salicylaldehydes, **HLa–e**, and of their novel  $Cu^{2+}$  complexes have been investigated. Analytical data, X-ray crystallography and EPR studies established that in the solid state the complexes are dimeric cationic species of formulae  $[Cu_2(N^H La-e)]Cl_4$ , whereas in solution they exist in the form of monomers of the type  $[Cu(N^H La-e)_2]Cl_2/[Cu(La-e)(N^H La-e)]Cl$  stabilized by solvent molecules. All ligands and the copper complex of **HLd** were shown to selectively inhibit AChE in the 4.61–9.31  $\mu M$  range. Results of docking and molecular dynamic studies suggest that the ligands are able to bind inside AChE in the same way known for AChE inhibitors, such as donepezil. Docking studies also showed that the complexes  $[Cu(N^H Ld)_2]^{2+}$  and  $[Cu(N^H Ld)(Ld)]^+$  are able to effectively bind to *EeAChE*. The dynamic of this binding, however, has not been investigated in this work and will be the subject of a future study. Considering that the high serum copper levels present in AD patients can trigger oxidative stress and cause neurotoxicity, we have investigated the  $Cu^{2+}$  chelating potential of **HLd** in HEPES at pH 6.6 and 7.4, in  $\mu M$  concentrations. UV–Vis spectrophotometric titrations confirmed formation of the 1:2 complex. Taking into account that neither **HLd** nor its  $Cu^{2+}$  complex was neurotoxic in mixed brain cultures and that **HLd** satisfies the criteria of the Lipinski's rule of 5 for CNS, our results suggest that the chelating compound **HLd** is promising as a multifunctional drug, by inhibiting AChE and, *via* complexation of

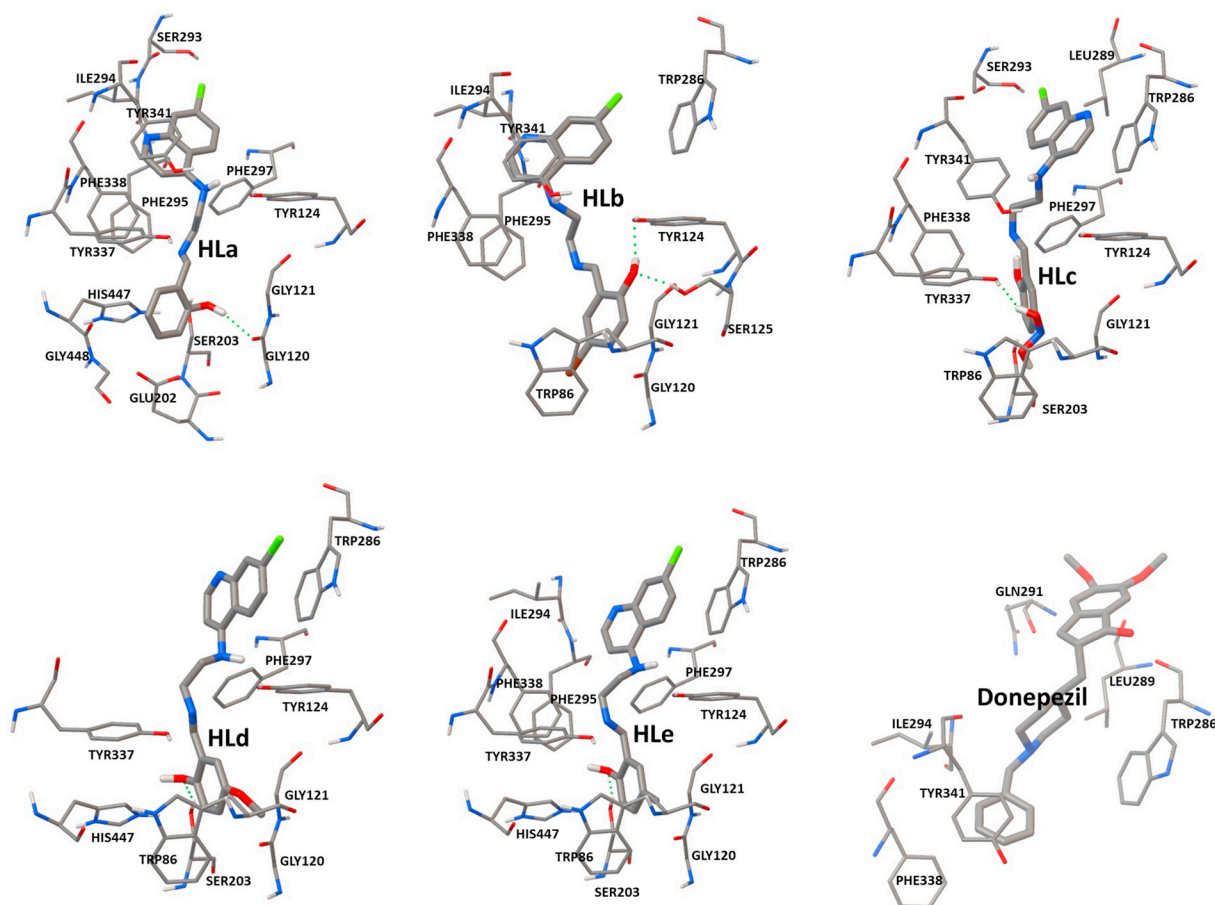


Fig. 5. Best poses obtained from the docking studies for ligands HLa–e and donepezil inside *EeAChE*.

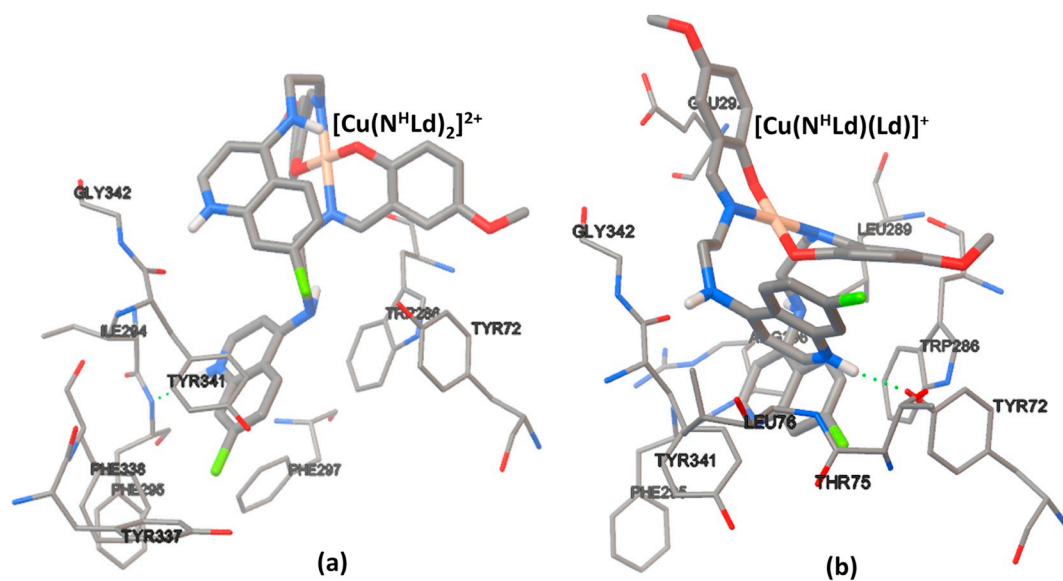


Fig. 6. Best poses of complexes  $[Cu(N^H Ld)_2]^{2+}$  (a) and  $[Cu(N^H Ld)(Ld)]^+$  (b) inside *EeAChE*.

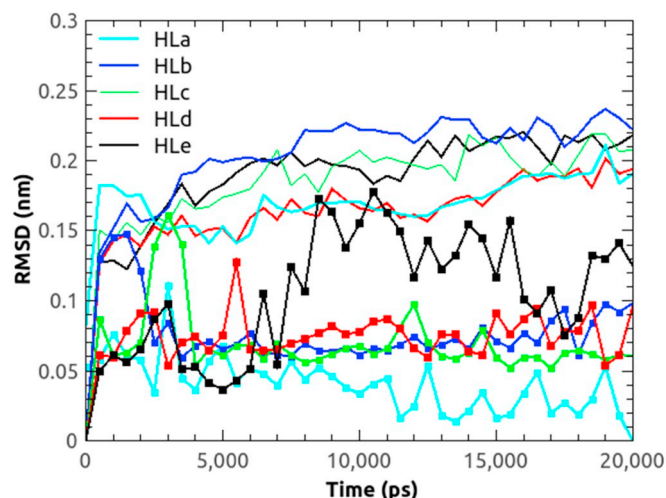


Fig. 7. RMSD plots for the systems *EeAChE*/ligands after 20.0 ns of MD simulation.

$\text{Cu}^{2+}$ , reducing neurotoxicity caused by oxidative stress. Further studies are in progress involving the design of other compounds with the 7-chloro-4-aminoquinoline nucleus, aiming at more efficient drugs for the treatment of AD.

## Abbreviations

AD	Alzheimer's disease
A $\beta$	amyloid- $\beta$
ADT	AutoDockTools
ACh	acetylcholine
AChE	acetylcholinesterase
<i>EeAChE</i>	AChE from <i>Electrophorus electricus</i>
<i>HssAChE</i>	human ( <i>Homo sapiens sapiens</i> ) AChE
BChE	butyrylcholinesterase
BSA	bovine serum albumin
ChEI	cholinesterase reversible inhibitor
COX2	cyclooxygenase-2
DMEM	Dulbecco's modified Eagle medium
FBS	fetal bovine serum
FDA	Food and Drug Administration
IL-1 $\beta$	Interleukin-1 beta
IL-6	Interleukin-6
MD	molecular dynamics
MTT	3-(4,5-dimethylthiazol-2-yl)-2,5-diphenyltetrazolium bromide
ROS	reactive oxygen species
RMSD	Root Mean Square Deviation
TNF- $\alpha$	Tumor Necrosis Factor alpha

## Acknowledgement

The authors gratefully acknowledge the Brazilian agencies National Council for Scientific and Technological Development (CNPq, grant numbers 306136/2011-2 – M.D.V. and 306156/2015-6 – T.C.C.F.), Coordenação de Aperfeiçoamento de Pessoal de Nível Superior - Brasil (CAPES, Finance Code 001 and V.S.Z. fellowship), National Institutes for Science and Technology (INCT-NT grant number 465346/2014-6 – F.R.S.L.) and the Rio de Janeiro Research Foundation (FAPERJ, grant numbers 26/201.352/2014 – M.D.V., 02/202.961/2017 – T.C.C.F. and post-doctoral fellowship – J.A.L.). We are grateful to the Molecular Spectroscopy (<http://www.uff.br/lame/>), NMR (<http://www.laremn.uff.br>) and X-Ray Diffraction (<http://www.lrx.uff.br>) Multiuser Laboratories at Universidade Federal Fluminense. We also thank the

free software developers (Linux, Gromacs, VMD, Qtplot, Xmgrace, etc.) who made our molecular modeling possible.

## Appendix A. Supplementary data

Crystallographic data for the structure have been deposited with the Cambridge Crystallographic Data Centre, CCDC No. 1502424 for compound  $[\text{Cu}_2(\text{N}^{\text{H}}\text{La-e})_4]\text{Cl}_4$ . Copies of this information may be obtained free of charge from the CCDC, 12 Union Road, Cambridge CB2 1EZ, UK (e-mail: [deposit@ccdc.cam.ac.uk](mailto:deposit@ccdc.cam.ac.uk) or [www: http://www.ccdc.cam.ac.uk](http://www.ccdc.cam.ac.uk)). Supplementary data to this article can be found online at <https://doi.org/10.1016/j.jinorgbio.2018.11.019>.

## References

- [1] M. Prince, A. Comas-Herrera, M. Knapp, G. Maëllenn, M. Karagiannidou, (2016) Alzheimer's Disease International (ADI), London, UK.
- [2] F.M. LaFerla, S. Oddo, Alzheimer's disease: Ab, tau and synaptic dysfunction, *Trends Mol. Med.* 11 (2005) 170–176.
- [3] D.M. Bowen, D. Neary, N.R. Sims, et al. (Eds.), *Adv. Behav. Biol.* 1st ed., I. Hanin (Ed.), 30 Plenum Press, New York, 1986, pp. 111–121.
- [4] L. Nilsson, A. Nordberg, J.A. Hardy, et al., *J. Neural Transm.* 67 (1986) 275–285.
- [5] P.T. Francis, A.M. Palmer, M. Snape, et al., *J. Neurol. Neurosurg. Psychiatry* 66 (1999) 137–147.
- [6] G.F. Chen, T.H. Xu, Y. Yan, et al., *Acta Pharmacol. Sin.* 38 (2017) 1205–1235.
- [7] W.J. Deardorff, E. Feen, G.T. Grossberg, *Drugs Aging* 32 (2015) 537–547.
- [8] C. Quintanova, R.S. Keri, S. Chaves, M.A. Santos, *J. Inorg. Biochem.* 151 (2015) 58–66.
- [9] M.I. Fernandez-Bachiller, C. Pérez, G.C. González-Muñoz, et al., *J. Med. Chem.* 53 (2010) 4927–4937.
- [10] R.S. Keri, C. Quintanova, S.M. Marques, et al., *Bioorg. Med. Chem.* 21 (2013) 4559–4569.
- [11] P. Camps, X. Formosa, C. Galdeano, et al., *J. Med. Chem.* 52 (2009) 5365–5379.
- [12] H. Dvir, D.M. Wong, M. Harel, et al., *Biochemist* 41 (2002) 2970–2981.
- [13] M. Kozurkova, S. Hamulakova, Z. Gazova, et al., *Pharmaceuticals* 4 (2011) 382–418.
- [14] A. Romero, J. Marco-Contelles, *Curr. Top. Med. Chem.* 17 (2017) 3328–3335.
- [15] M. Ventriglia, S. Bucossi, V. Panetta, et al., *J. Alzheimers Dis.* 30 (2012) 981–984.
- [16] S.A. James, I. Volitakis, P.A. Adlard, J.A. Duce, C.L. Masters, R.A. Cherny, A.I. Bush, *Free Radic. Biol. Med.* 52 (2012) 298–302.
- [17] C. Cheignona, M. Tomasa, D. Bonnefont-Rousselot, et al., *Redox Biol.* 14 (2018) 450–464.
- [18] E.E. Tuppo, H.R. Arias, *Int. J. Biochem. Cell Biol.* 37 (2005) 289–305.
- [19] M.T. Heneka, M.K. O'Banion, *J. Neuroimmunol.* 184 (2007) 69–91.
- [20] L.E. Rojo, J.A. Fernández, A.A. Maccioni, et al., *Arch. Med. Res.* 39 (2008) 1–16.
- [21] J.A. Lima, T.W.R. Costa, L.L. Silva, et al., *An. Acad. Bras. Cienc.* (2015) 1–12.
- [22] L. Glans, A. Ehnbo, C. Kock, et al., *Dalton Trans.* 41 (2012) 2764–2773.
- [23] E. Ekengard, L. Glans, I. Cassells, et al., *Dalton Trans.* 44 (2015) 19314–19329.
- [24] M.V. de Souza, K.C. Pais, C.R. Kaiser, et al., *Bioorg. Med. Chem.* 17 (2009) 1474–1480.
- [25] B.A. Solaja, D. Opsenica, K.S. Smith, et al., *Med. Chem.* 51 (2008) 4388–4391.
- [26] V.R. Solomon, S.K. Puri, K. Srivastava, et al., *Bioorg. Med. Chem.* 13 (2005) 2157–2165.
- [27] S. Stoll, A. Schweiger, *J. Magn. Reson.* 178 (2006) 42–55.
- [28] G.M. Sheldrick, *Acta Cryst A64* (2008) 112–122.
- [29] G.M. Sheldrick, *Acta Cryst C71* (2015) 3–8.
- [30] L.J. Bourhis, O.V. Dolomanov, R.J. Gildea, et al., *Acta Cryst A71* (2015) 59–75.
- [31] O.V. Dolomanov, L.J. Bourhis, R.J. Gildea, et al., *Appl. Cryst.* 42 (2009) 339–341.
- [32] (a) CELL\_NOW. Version 2008/4. Georg-August-Universität Göttingen, Göttingen, Germany.  
(b) Bruker, TWINABS, Bruker AXS Inc., Madison, Wisconsin, USA, 2001
- [33] A.L. Spek, *Acta Cryst C71* (2015) 9–18.
- [34] J.A. Lima, R.S. Costa, R.A. Epifânio, et al., *Pharmacol. Biochem. Behav.* 92 (2009) 508–513.
- [35] G.L. Ellman, K.D. Courtney, J.R.V. Andres, et al., *Biochem. Pharmacol.* 7 (1961) 88–95.
- [36] F.R. Lima, C.P. Arantes, A.G. Muras, et al., *J. Neurochem.* 103 (2007) 2164–2176.
- [37] R.S. Gardner, *Anal. Biochem.* 59 (1974) 272–276.
- [38] A.C.C. da Fonseca, L. Romão, R.F. Amaral, et al., *Neuroscience* 200 (2012) 130–141.
- [39] G.M. Morris, R. Huey, W. Lindstrom, et al., *J. Comput. Chem.* 16 (2009) 2785–2791.
- [40] S. Pronk, S. Pall, R. Schulz, et al., *Bioinformatics* 29 (2013) 845–854.
- [41] A.K. Malde, L. Zuo, M. Breeze, et al., *J. Chem. Theory Comput.* 7 (2011) 4026–4037.
- [42] G. Bussi, D. Donadio, M. Parrinello, *J. Chem. Phys.* 126 (2007) (014101(1–7)).
- [43] U. Essmann, L. Pereira, M.L. Berkowitz, et al., *J. Chem. Phys.* 103 (1995) 8577–8593.
- [44] M. Parrinello, A. Rahman, *J. Appl. Phys.* 52 (1981) 7182–7190.
- [45] B.S. Creaven, M. Devereux, D. Karcz, et al., *J. Inorg. Biochem.* 103 (2009) 1196–1203.

- [46] P. Pattanayak, J.L. Pratihari, D. Patra, et al., *J. Coord. Chem.* 66 (2013) 568–579.
- [47] P.K. Bhaumik, K. Harms, S. Chattopadhyay, *Polyhedron* 62 (2013) 179–187.
- [48] C.H. Kaschula, T.J. Egan, R. Hunter, et al., *J. Med. Chem.* 45 (2002) 3531–3539.
- [49] A.W. Addison, T.N. Rao, J. Reedijk, et al., *J. Chem. Soc. Dalton Trans.* (1984) 1349–1356.
- [50] G.R. Clark, J.M. Waters, T.N. Waters, *J. Inorg. Nucl. Chem.* 39 (1977) 1971–1975.
- [51] T.V. Sydoruk, E.A. Buvaylo, V.N. Kozozay, et al., *Acta Crystallogr. Sect. E: Struct. Rep. Online* 69 (2013) m551–m552.
- [52] Y.L. Sang, X.S. Lin, *Russ. J. Coord. Chem.* 36 (2010) 472–476.
- [53] M. Tümer, *J. Coord. Chem.* 60 (2007) 2051–2065.
- [54] H. Yokoi, A. Takaeuchi, S. Yamada, *Bull. Chem. Soc. Jpn.* 58 (1985) 2990–2994.
- [55] J. Jezierska, B. Jeżowska-Trzebiatowska, G. Petrova, *Inorg. Chim. Acta* 50 (1981) 153–157.
- [56] M. Chikira, T. Isobe, *Bull. Chem. Soc. Jpn.* 45 (1972) 3006–3011.
- [57] J. Peisach, W.E. Blumberg, *Arch. Biochem. Biophys.* 165 (1974) 691–708.
- [58] W.J. Geary, *Coord. Chem. Rev.* 7 (1971) 81–122.
- [59] M. Ikram, S.U. Rehman, S. Rehman, et al., *Inorg. Chim. Acta* 390 (2012) 210–216.
- [60] A.L.F. Sarria, A.F.L. Vilela, B.M. Frugeri, et al., *J. Inorg. Biochem.* 164 (2016) 141–149.
- [61] Z.-M. Wang, P. Cai, Q.-H. Liu, et al., *Eur. J. Med. Chem.* 123 (2016) 282–297.
- [62] C.A. Lipinski, F. Lombardo, B.W. Dominy, et al., *Adv. Drug Deliv. Rev.* 64 (2012) 4–17.
- [63] H. Pajouhesh, G.R. Lenz, *NeuroRx* 2 (2005) 541–553.
- [64] ChemOffice, CambridgeSoftCorporation, Cambridge, USA, 2009.
- [65] M. Kontoyanni, L.M. McClellan, G.S. Sokol, *J. Med. Chem.* 47 (2004) 558–565.
- [66] D.C.F. Neto, J.A. Lima, J.S.F.D. Almeida, et al., *J. Biomol. Struct. Dyn.* 7 (2017) 1–15.
- [67] J. Cheung, M.J. Rudolph, F. Burshteyn, et al., *J. Med. Chem.* 55 (2012) 10282–10286.
- [68] M.R. Ali, M. Sadoqi, S.G. Møller, et al., *J. Mol. Graph. Model.* 76 (2017) 36–42.